



HAL
open science

Facile and Scalable Preparation of Ruthenium Oxide-Based Flexible Micro-Supercapacitors

Kevin Brousse, Sébastien Pinaud, Son Nguyen, Pier-Francesco Fazzini, Raghda Makarem, Claudie Josse, Yohann Thimont, Bruno Chaudret, Pierre-Louis Taberna, Marc Respaud, et al.

► **To cite this version:**

Kevin Brousse, Sébastien Pinaud, Son Nguyen, Pier-Francesco Fazzini, Raghda Makarem, et al.. Facile and Scalable Preparation of Ruthenium Oxide-Based Flexible Micro-Supercapacitors. *Advanced Energy Materials*, 2020, 10 (6), pp.1903136. 10.1002/aenm.201903136 . hal-02498675

HAL Id: hal-02498675

<https://hal.science/hal-02498675>

Submitted on 4 Mar 2020

HAL is a multi-disciplinary open access archive for the deposit and dissemination of scientific research documents, whether they are published or not. The documents may come from teaching and research institutions in France or abroad, or from public or private research centers.

L'archive ouverte pluridisciplinaire **HAL**, est destinée au dépôt et à la diffusion de documents scientifiques de niveau recherche, publiés ou non, émanant des établissements d'enseignement et de recherche français ou étrangers, des laboratoires publics ou privés.







Open Archive Toulouse Archive Ouverte (OATAO)

OATAO is an open access repository that collects the work of Toulouse researchers and makes it freely available over the web where possible

This is an author's version published in: <http://oatao.univ-toulouse.fr/25564>

Official URL: <https://doi.org/10.1002/aenm.201903136>

To cite this version:

Brousse, Kevin  and Pinaud, Sébastien and Nguyen, Son and Fazzini, Pier-Francesco and Makarem, Raghda and Josse, Claudie and Thimont, Yann  and Chaudret, Bruno and Taberna, Pierre-Louis  and Respaud, Marc and Simon, Patrice  *Facile and Scalable Preparation of Ruthenium Oxide-Based Flexible Micro-Supercapacitors*. (2020) *Advanced Energy Materials*, 10 (6). 1903136. ISSN 1614-6832

Any correspondence concerning this service should be sent to the repository administrator: tech-oatao@listes-diff.inp-toulouse.fr

Facile and Scalable Preparation of Ruthenium Oxide-Based Flexible Micro-Supercapacitors

Kévin Brousse, Sébastien Pinaud, Son Nguyen, Pier-Francesco Fazzini, Raghda Makarem, Claudie Josse, Yohann Thimont, Bruno Chaudret, Pierre-Louis Taberna, Marc Respaud, and Patrice Simon**

Tremendous efforts have been invested in the development of the internet of things during the past 10 years. Implantable sensors still need embedded miniaturized energy harvesting devices, since commercialized thin films and microbatteries do not provide sufficient power densities and suffer from limited lifetime. Therefore, micro-supercapacitors are good candidates to store energy and deliver power pulses while providing non-constant voltage output with time. However, multistep expensive protocols involving mask aligners and sophisticated cleanrooms are used to prepare these devices. Here, a simple and versatile laser-writing procedure to integrate flexible micro-supercapacitors and microbatteries on current-collector-free polyimide foils is reported, starting from commercial powders. Ruthenium oxide (RuO₂)-based micro-supercapacitors are prepared by laser irradiation of a bilayered tetrachloroauric acid (HAuCl₄·3H₂O)–cellulose acetate/RuO₂ film deposited by spin-coating, which leads to adherent Au/RuO₂ electrodes with a unique pillar morphology. The as-prepared microdevices deliver 27 mF cm⁻²/540 F cm⁻³ in 1 M H₂SO₄ and retain 80% of the initial capacitance after 10 000 cycles. This simple process is applied to make carbon-based micro-supercapacitors, as well as metal oxide based pseudocapacitors and battery electrodes, thus offering a straightforward solution to prepare low-cost flexible microdevices at a large scale.

1. Introduction

Smart wearable systems have attracted a growing interest in the past years to support the development of sensor networks and communicating objects called the internet of things (IoT). IoT is a generic term used to describe the exchange of data between portable, smart, and connected devices creating a new range of devices able to interact and communicate through the internet.^[1,2] Applications relying on wearable devices such as healthcare, smart clothes, or electronic papers have motivated many research works to achieve for instance individual management and continuous monitoring of patients.^[3] Reliable microsized energy storage sources (ESS) such as batteries and electrochemical capacitors (ECs) are needed to power these devices.^[4–7] ECs and batteries are complementary ESS covering a broad range of applications. While batteries can deliver low power for long time (10s of hours), ECs are suitable for delivering high peak current or power for short times (up to 10s of seconds), making them promising candidates to power

Dr. K. Brousse, Dr. Y. Thimont, Dr. P. L. Taberna, Prof. P. Simon
Université Paul Sabatier
Laboratoire CIRIMAT
UMR CNRS 5085, 118 route de Narbonne, 31062 Toulouse, France
E-mail: simon@chimie.ups-tlse.fr

Dr. K. Brousse, Dr. P. L. Taberna, Prof. P. Simon
Réseau sur le Stockage Electrochimique de l'Energie
FR CNRS n°3459, France

S. Pinaud, Dr. S. Nguyen, Dr. P. F. Fazzini, Dr. R. Makarem,
Dr. B. Chaudret, Prof. M. Respaud
Université de Toulouse
LPCNO
UMR 5215 INSA-UPS-CNRS
31077 Toulouse, France
E-mail: respaud@insa-toulouse.fr

S. Pinaud, Dr. S. Nguyen, Dr. P. F. Fazzini, Dr. R. Makarem,
Dr. B. Chaudret, Prof. M. Respaud
Institut National des Sciences Appliquées
135 avenue de Rangueil, 31077 Toulouse, France

Dr. P. F. Fazzini, Dr. R. Makarem, Prof. M. Respaud
AIME
Université de Toulouse
INSA
UPS
INP
135 avenue de Rangueil, 31077 Toulouse, France

C. Josse
Centre de Microcaractérisation Raimond Castaing (CNRS UMS 3623)
Université Fédérale de Toulouse
31400 Toulouse, France

smart wearable systems.^[8,9] Screen printing of carbon,^[10] pseudo-capacitive materials,^[11–13] or stamping processes,^[14] were reported with limited areal capacitance ($<20 \text{ mF cm}^{-2}$) or resolution. Similarly, microdevices prepared from atomic layer deposition,^[15] reactive sputtering,^[16] and electron beam evaporation techniques suffer from a poor areal capacitance (few mF cm^{-2}),^[17] due to the small electrode thicknesses ($<100 \text{ nm}$).

Wet processing routes, such as electrodeposition or electropolymerization,^[18–20] are suitable for preparing thick electrodes ($>50 \text{ }\mu\text{m}$) on flexible substrates with capacitance exceeding 10 mF cm^{-2} . However, these multistep wet processing routes are not fully compatible with the techniques used in the semiconductor industry and are therefore difficult to upscale.

Laser-writing process focused a lot of interest these past years for preparing electrodes for energy storage applications. Following pioneer work from Arnold et al.,^[21] laser irradiation was used to reduce graphite oxide (GO) into laser-scribed graphene (LSG),^[22] or to achieve direct conversion of polyimide (PI) substrates into laser-induced graphene (LIG) with a limited areal capacitance ($<20 \text{ mF cm}^{-2}$).^[23–26]

Ruthenium oxide exhibits one of the highest gravimetric capacitance (1450 F g^{-1}) together with decent electrical conductivity (from 4 to 46 S cm^{-1} depending on the hydration rate of RuO_2).^[27] Since the realization of micro-supercapacitors requires only a limited amount of RuO_2 , typically less than 1 mg cm^{-2} , the cost is not that much an issue.^[28] Therefore, Kaner's group recently adapted their GO laser-scribing method to prepare LSG/ RuO_2 -based flexible micro-supercapacitors from GO/ RuCl_3 mixture.^[29] Laser irradiation of the mixture coated onto flexible substrate led to simultaneous reduction of GO into LSG and Ru(III) oxidation into Ru(IV) . However, the small RuO_2 weight loading achieved by this method—about $90 \text{ }\mu\text{g cm}^{-2}$ —limited the areal and volumetric capacitance of the device to 10 mF cm^{-2} and 11 F cm^{-3} , respectively, in $1 \text{ M H}_2\text{SO}_4$ (estimated from Ragone plot). In addition, such oxidation dependent process is not convenient for the preparation of every carbon- (microporous carbon), metal oxide- (Nb_2O_5 , MnO_2 , e.g., for which a specific morphology has to be obtained), or LiFePO_4 , as the final active material is obtained from the transformation of a precursor under the laser beam. Differently, the present work reports about the preparation of RuO_2 -based micro-supercapacitors from the direct laser-writing of a commercial $\text{RuO}_2 \cdot x\text{H}_2\text{O}$ powder containing ink spin-coated onto an electrically insulating flexible polyimide film, which does not need the design of masks or controlled atmospheres. This process, which results in the preparation of stable electrodes with improved mechanical properties, can be extended to other materials such as metal oxides, carbons, or phosphates to design a large variety of microdevices for various applications.

2. Results

2.1. Preparation of RuO_2 -Based Flexible Micro-Supercapacitors on Current-Collector-Free Polyimide Foil

Figure 1 shows the fabrication process of the RuO_2 -based micro-supercapacitors onto a current-collector-free PI flexible

substrate. An ink containing a mixture of a tetrachloroauric acid ($\text{HAuCl}_4 \cdot 3\text{H}_2\text{O}$) gold precursor and cellulose acetate dissolved in tetrahydrofuran (THF) is spin-coated onto the flexible substrate (layer 1). In a second step, a $\text{RuO}_2 \cdot 1.8\text{H}_2\text{O}$ commercial powder dispersed in THF is deposited by spin-coating (layer 2) onto the layer 1. The details of the ink formulations are given in Section 3. Then, laser-writing was performed on the bilayered $\text{HAuCl}_4 \cdot 3\text{H}_2\text{O}$ -cellulose acetate/ RuO_2 film. After washing in acetone and ethanol, mechanically stable patterned electrodes adhering to the flexible PI film were obtained.

The $\text{HAuCl}_4 \cdot 3\text{H}_2\text{O}$ -containing transition layer 1 was found to be the key to promote adherence of the final RuO_2 layer onto the insulating flexible substrate. Simulation of the heat induced by the laser beam was performed using Comsol Multiphysics software (details in Supporting Information). It was found that the presence of both $\text{HAuCl}_4 \cdot 3\text{H}_2\text{O}$ and cellulose acetate is necessary, as $\text{HAuCl}_4 \cdot 3\text{H}_2\text{O}$ allows to absorb the laser energy (Figure S1, Supporting Information), leading to the pyrolysis of the cellulose acetate within the film, thus resulting in the formation of Au ($T > 180 \text{ }^\circ\text{C}$) on both side of the laser path over $100 \text{ }\mu\text{m}$ (Figure S2a–f, Supporting Information). Indeed, in the absence of the intermediate $\text{HAuCl}_4 \cdot 3\text{H}_2\text{O}$ layer, the laser-scribed RuO_2 did not show any adherence on PI/Ti/Au substrates (Figure S3, Supporting Information). The mechanisms involved during the laser-writing are schematically illustrated in Figure 1. The influence of the $\text{HAuCl}_4 \cdot 3\text{H}_2\text{O}$ content in the layer 1—starting from 33wt%, as below this content, the electrodes could not be successfully prepared because of lack of adherence onto the substrate—on the electrochemical performance of the laser-scribed RuO_2 -based electrodes was studied by cyclic voltammetry using PI films coated with a Ti/Au thin film as current collector (Figure S4, Supporting Information). The cyclic voltammograms (CV) recorded at 20 mV s^{-1} show pseudocapacitive shapes (Figure S5A, Supporting Information), with two cathodic and anodic bumps, which is characteristic of the electrochemical signature of pseudocapacitive RuO_2 .^[30] The highest capacitance of 410 mF cm^{-2} was achieved in sulfuric acid for the laser-scribed electrode with a content of 80wt% of $\text{HAuCl}_4 \cdot 3\text{H}_2\text{O}$ in layer 1 (Figure S5B, Supporting Information), as a result of the increase of the deposited mass of RuO_2 (Figure S5C, Supporting Information). Importantly, the mass loading obtained here is higher than the one calculated for LSG/ RuO_2 electrodes prepared by the oxidation of a RuCl_3 precursor.^[29] This composition was selected to prepare the microdevice in Figure 1 on current-collector-free PI.

2.2. Characterization of the Laser-Scribed RuO_2 Electrodes

Scanning electron microscopy (SEM) images (obtained using secondary electrons), representative of the as-prepared laser-scribed RuO_2 electrodes onto current-collector-free substrate reveal that the film covers the flexible substrate entirely (Figure 2A). The deposit grows as small crystals and some popcorn-like structures can also be locally observed, accounting for about 20% of the total surface (Figure 2B). These crystals form a homogeneous and dense structure onto the substrate as observed in Figure 2C (top view) and Figure 2D (cross section). In Figure 2E is shown a cross-sectional view obtained using SEM in backscattered electrons mode, representative of the deposit, which reveals the

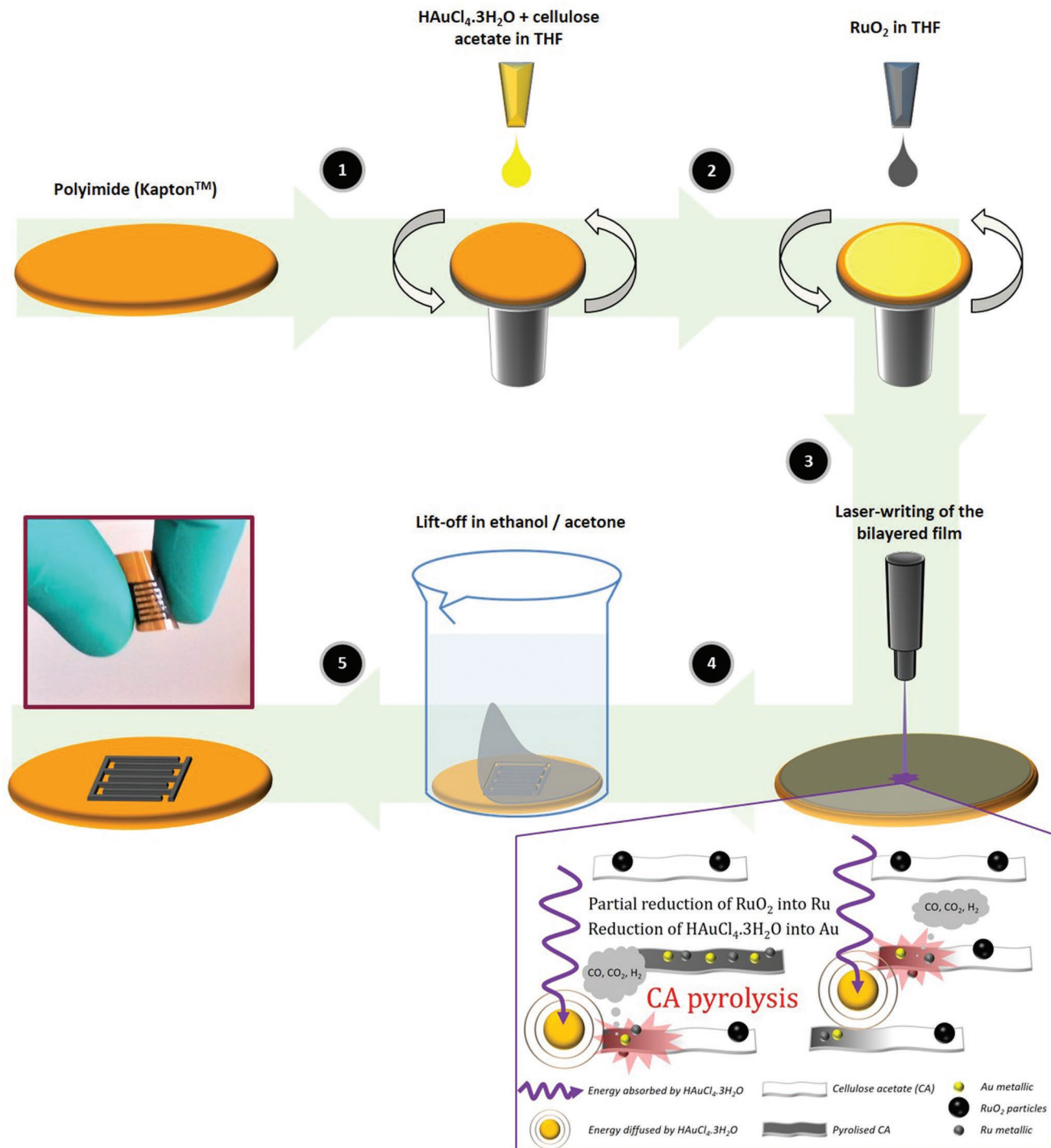


Figure 1. Fabrication process of RuO₂-based flexible micro-supercapacitors. HAuCl₄·3H₂O–cellulose acetate mixture (1) and RuO₂ (2) are dispersed in THF and successively spin-coated on polyimide. Laser-writing is performed on the as-deposited bilayered film (3) and the non-exposed areas are removed by washing with ethanol and acetone (4) to reveal the interdigitated electrodes (5).

bilayered aspect of the deposit (the tilt angle between the observation axis and the specimen surface is 54°). The popcorns start to grow from the RuO₂ crystals; such structure might be due to a local overheating during the laser-writing process. Energy dispersive X-ray spectrometer (EDX) mapping shows the presence

of oxygen and ruthenium in both layers, but it can be clearly observed that the oxygen concentration is much higher in the 500 nm-thick layer containing the pillars (Figure 2F), in comparison with the thin interface layer at the PI film/RuO₂ pillars. This suggests that the upper layer is composed by RuO₂ while

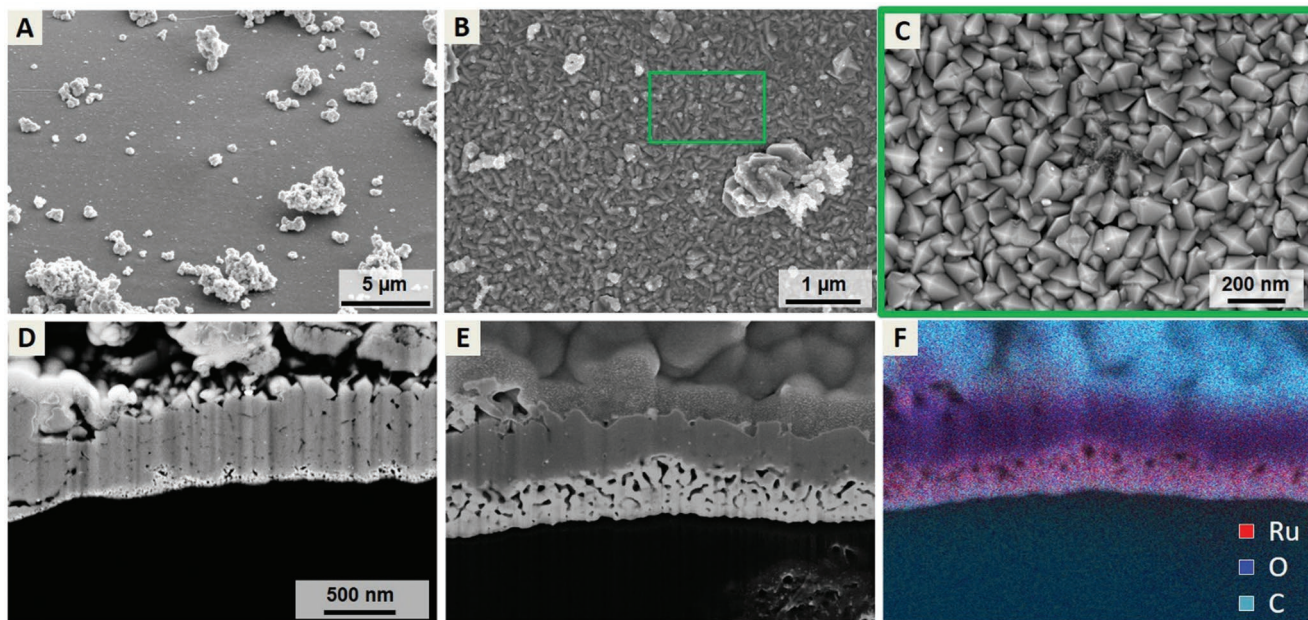


Figure 2. Structure of the Au/RuO₂ growing under laser beam. A) Tilted, and B) top view of the Au/RuO₂ deposited on polyimide (PI), and C) zoom on the RuO₂ crystals. D) Cross-sectional view of the PI/laser-scribed Au/RuO₂ with E) tilted SEM image obtained using backscattered electrons and F) the corresponding EDX map evidencing the presence of Ru at the interface. The large 54° tilt angle used in (E,F) to highlight the porous layer prevent from using reliable scale bar.

the lower one could be mainly composed by metallic Ru. In addition, Figure S6A, Supporting Information, shows that several Au nanoparticles are visible in the RuO₂ layers, which are likely to enhance the electrical conductivity of the RuO₂. XRD (X-ray diffraction) measurements confirmed the presence of crystalline RuO₂ (Figure S6B, Supporting Information) as well as Au and Ru metals, which is compatible with the presence of a metallic Ru/RuO₂ stack suggested by the EDX maps. These observations confirm the mechanism proposed, where H₂AuCl₄ adsorbs the energy of the laser during laser-writing, resulting in the pyrolysis of the cellulose acetate and formation of metallic Au in the first layer. As reported by Collard et al., the pyrolysis of cellulose involves the superposition of several pathways (char formation, depolymerization, and fragmentation), leading to the generation of CO₂ and CO (as well as H₂ for temperatures higher than 500 °C).^[31] In addition, the carbon-containing pyrolysis products and the reductive atmosphere generated further induce the partial reduction of RuO₂ into Ru (Figure 1), in agreement with the reduction of Ru(+III) by CO in RuCl₃/cellulose acetate films.^[32] Such a reduction has been previously reported for RuO₂ thin films prepared from laser-writing of Ru(COD)(COT).^[33]

The TEM cross-sectional view presented in Figure 3A gives a local perspective of the crystalline structure observed by SEM. Some rare “popcorn-like” structures starting from a dense layer containing small pillars lying on a thin porous layer (Figure 3B) are dispersed on the surface. Figure 3B as well as the high-resolution TEM of the RuO₂ /PI substrate interface presented in Figure 3C show that the first 100 nm-thick porous layer contains particles randomly oriented. The Fourier transform of well oriented particles of the image in Figure 3C, displayed in inset, shows that the crystalline structure of the single particles is compatible with the structure of metallic Ru (hexagonal compact P63/mmc

$a = b = 270$ pm, $c = 427.5$ pm). Inside the pillars, single crystal patterns are obtained in this region, indicating that the process induced a monocrystalline growth, mainly composed by RuO₂, with the presence of Ru inclusions. Indeed, Fourier analysis performed on different particles inside the pillar region shows patterns compatible both with tetragonal RuO₂ (quadratic P4/2mm $a = b = 452$ pm, $c = 311.6$ pm) and hexagonal Ru (Figure 3D and Figure 3E, respectively). Surface faceting is another indication of the regular and monocrystalline character of the pillar growth. However, the presence of several nanoparticles on top of them prevents a precise identification (Figure 3F). It is worth mentioning that Au nanoparticles were also found in the porous layer (EDX analysis; Figure S7A,B, Supporting Information). In summary, the laser-writing of the bilayered H₂AuCl₄·3H₂O–cellulose acetate/RuO₂ leads to a 500 nm-thick deposit containing a layer of metallic Ru, and a second layer of Ru/RuO₂ pillars (Figure S7C,D, Supporting Information) embedding Au nanoparticles.

2.3. Electrochemical Characterization of the RuO₂-Based Flexible Micro-Supercapacitors

As shown in Figure 4A, the laser-writing process which has been developed (Figure 1) could be extended for the realization of 36 flexible micro-supercapacitors, on a 10 cm-diameter current-collector-free polyimide foil, without any short-circuited device, thus making this work promising for the preparation of flexible micro-supercapacitors at a large scale. Interestingly, the geometry of the electrodes prepared from the precedent process could be easily tuned, thanks to this facile fabrication process (Figure S8A, Supporting Information), without the use of any mask design or additional photolithography step, which allows

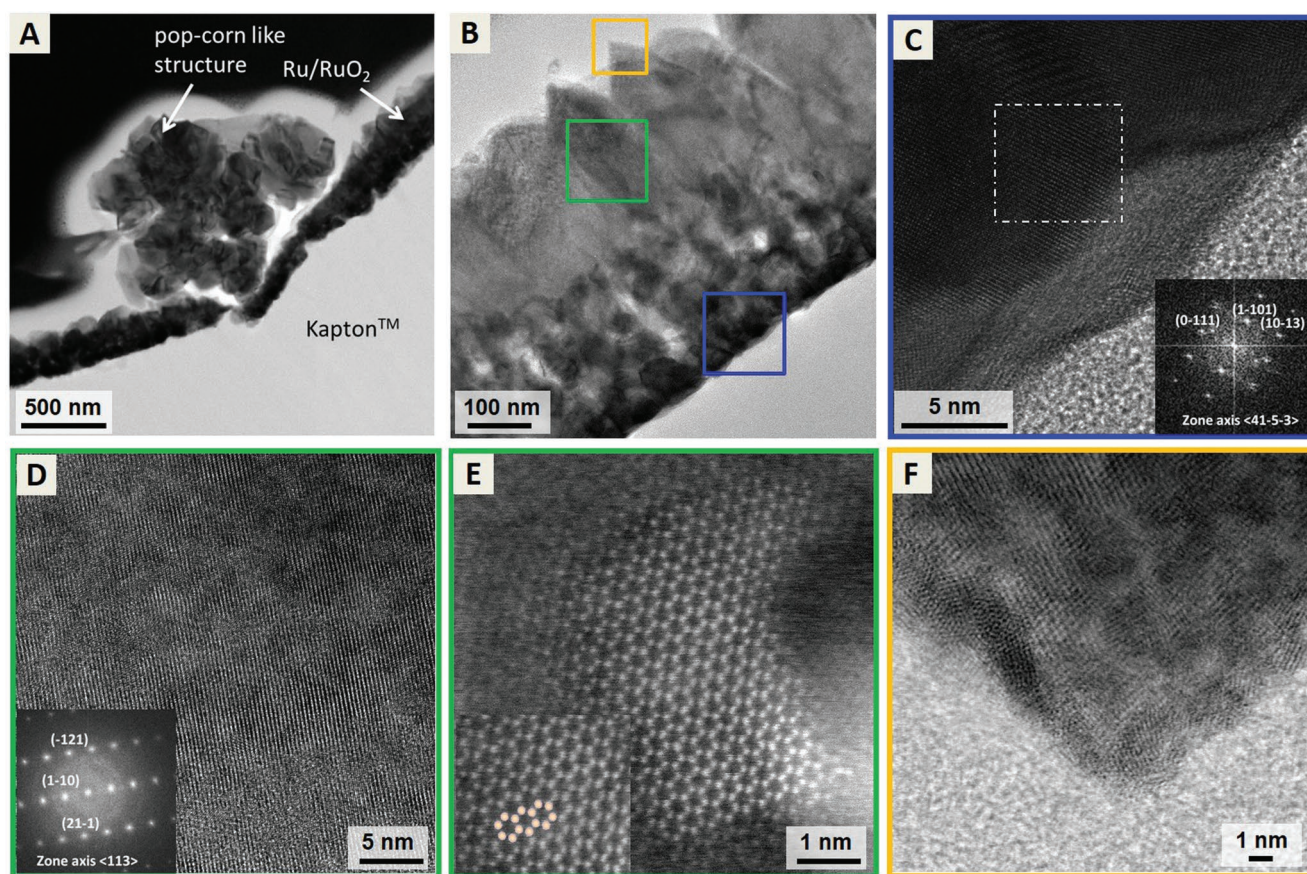


Figure 3. Observation of the polyimide/RuO₂ interface. A) TEM image of a popcorn-like structure grown on B) the Ru/RuO₂ at the interface with the flexible substrate. C) High-resolution TEM image of the RuO₂/PI interface; the inset shows the Fourier transform of the image in the dotted rectangle. D) Morphology of the RuO₂, with a Fourier transform of the full image as an inset and E) Ru contained in the pillars (the inset shows the superposition of the hexagonal ruthenium structure in a <0001> orientation and a region of the image). F) Bright-field TEM observation of the top of the pillars.

to prepare micro-supercapacitors assembled in series to power a commercial light emitting diode (Figure S8B–D, Supporting Information). Figure 4B presents the CV recorded in 1 M H₂SO₄ at 5 mV s⁻¹ for a RuO₂/Au micro-supercapacitor shown in inset (four 500 μm large and 5 mm long fingers per polarity, separated by 500 μm large interspaces). The pseudocapacitive behavior of RuO₂ electrodes can be seen through the rectangular shape; 27 mF cm⁻²/540 F cm⁻³ of device were delivered by the interdigitated micro-supercapacitor, which challenges the best flexible micro-supercapacitors reported so far.^[13,17,29,34–39] The energy density delivered by these flexible micro-supercapacitors reached 3.1 μWh cm⁻², which is above the state-of-the-art of flexible interdigitated micro-supercapacitors (Figure S9, Supporting Information). Although being current-collector-free devices, power performance of our micro-supercapacitors is similar to those reported in the literature. Furthermore, the flexible micro-supercapacitor exhibited good cycling abilities, with 80% of the initial capacitance delivered after 10 000 cycles carried out at 100 mV s⁻¹ (Figure 4C). The slight decrease of the capacitance during the first 1000 cycles was attributed to the release of loosely attached RuO₂ particles. The use of a gel electrolyte, such as polyvinylalcohol (PVA)–H₂SO₄, is expected to prevent such capacitance decrease upon cycling. In addition, galvanostatic charge/discharge experiments were carried out (Figure S10,

Supporting Information), and typical linear plots were observed, even at a low current density of 0.3 mA cm⁻². Indeed, the absence of significant leakage current (3 μA at 1 V) on the cyclic voltammogram presented in Figure 4B allows to test the as-prepared micro-supercapacitor at low scan rates (5 mV s⁻¹) or current densities (0.3 mA cm⁻²), which is not possible for LIG-based and LSG/RuO₂-based microdevices.^[22,23,29] Alternatively to the high energy design, high power micro-supercapacitors can be prepared by tuning the process to prepare thin-film electrodes, once again avoiding the use of Ti/Au current collectors (see Supporting Information). Such strategy leads to a low areal capacitance (5 mF cm⁻² of device, 20 mF cm⁻² of electrode) but high power performance, as shown in Figure 4D, since such microdevice can withstand a scan rate of up to 1 V s⁻¹ with almost no voltammogram distortion. The Nyquist plot recorded at the open circuit voltage shows a typical pseudocapacitive behavior with a sharp increase of the imaginary part of the impedance at low frequencies (Figure 4E). The small-depressed semicircle observed at high frequencies is associated with the contact impedance at the polyimide substrate/electrode interface. A cell series resistance of 3.5 Ω cm² was measured at high frequencies, which remains low considering the absence of any current collector, resulting in high power performance with a capacitance retention of about 60% at 1 V s⁻¹ (Figure 4F).

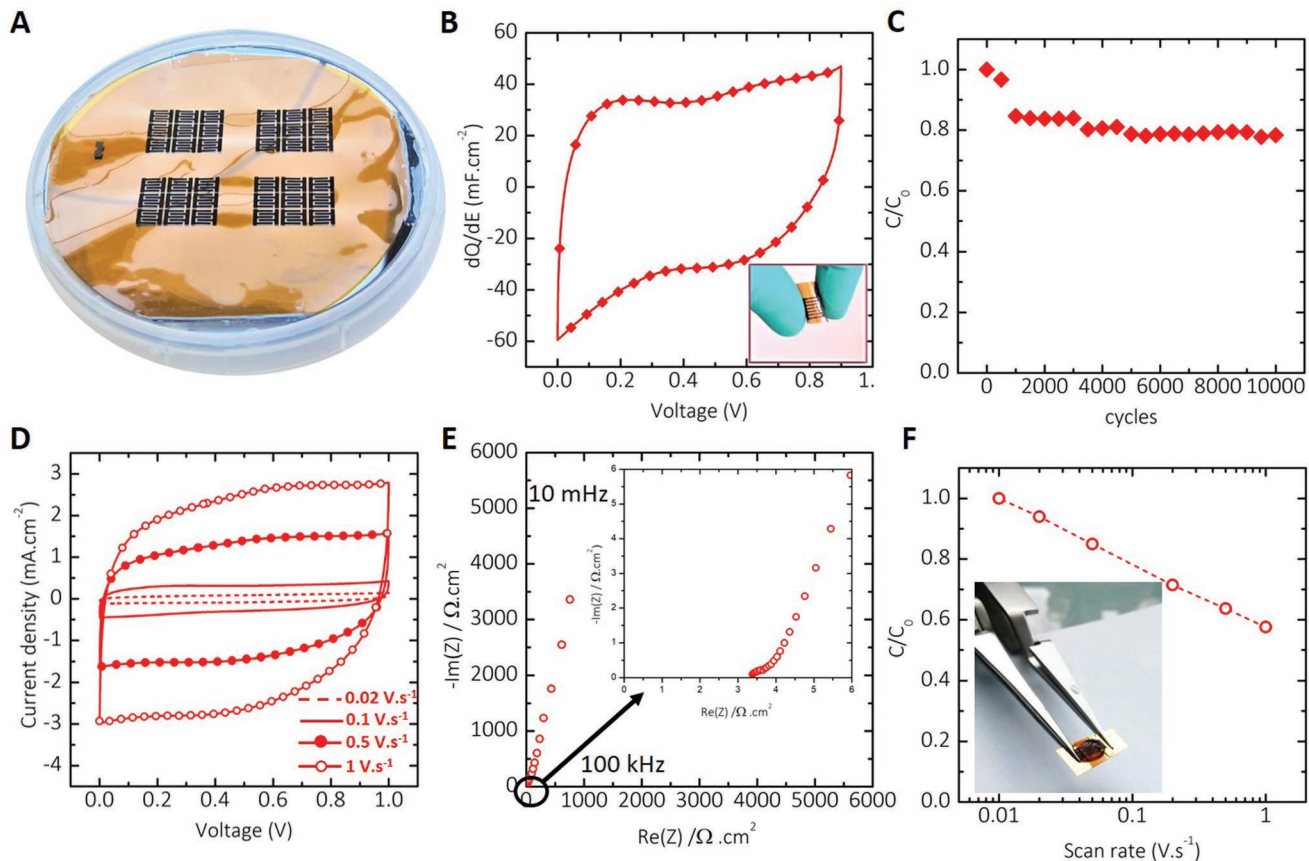


Figure 4. Laser-writing of flexible RuO_2/Au micro-supercapacitors. A) Integration of 36 micro-supercapacitors on polyimide sheet. B) Cyclic voltammograms of a RuO_2/Au flexible micro-supercapacitor recorded at 5 mV s^{-1} in $1 \text{ M H}_2\text{SO}_4$ and C) the corresponding capacitance retention of the device over 10 000 cycles. D) Cyclic voltammogram of a RuO_2/Au flexible micro-supercapacitor (power design) at various scan rate, E) the corresponding Nyquist plot, and F) change of the areal capacitance with the scan rate.

Besides, cyclic voltammetry was performed on bended RuO_2/Au micro-supercapacitors ($1 \text{ M H}_2\text{SO}_4$, bending angle of 120°). The cyclic voltammogram obtained at 20 mV s^{-1} (**Figure 5A**) is

similar to the one of a flat microdevice, thus confirming the good adherence of the laser-scribed material, as well as the flexibility of the as-prepared micro-supercapacitors. Finally, a $\text{PVA-H}_2\text{SO}_4$

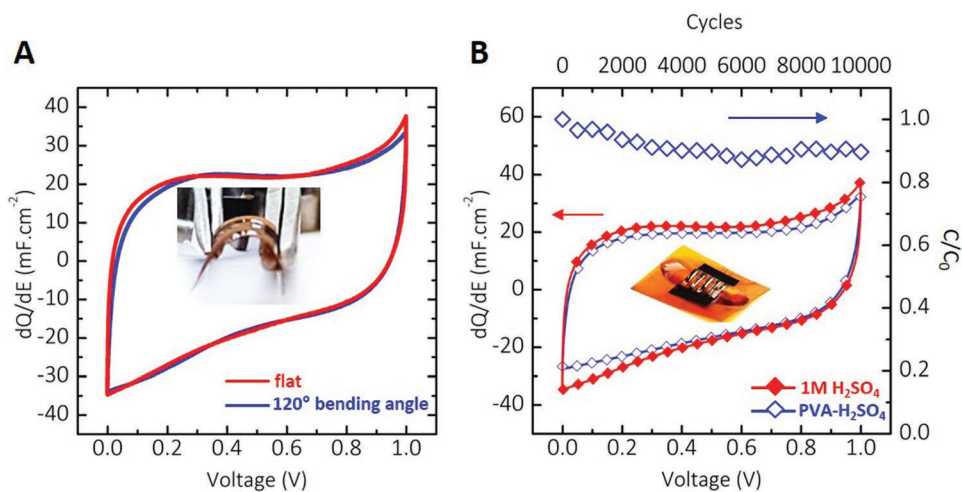


Figure 5. Flexible and all-solid-state RuO_2 -based micro-supercapacitors. A) Cyclic voltammograms of a flat and a bended RuO_2/Au micro-supercapacitor recorded at 20 mV s^{-1} in $1 \text{ M H}_2\text{SO}_4$. B) Cyclic voltammograms of a RuO_2/Au micro-supercapacitor recorded at 20 mV s^{-1} in $1 \text{ M H}_2\text{SO}_4$ and $\text{PVA-H}_2\text{SO}_4$ solid electrolyte, and the corresponding capacitance retention (top and right axes).

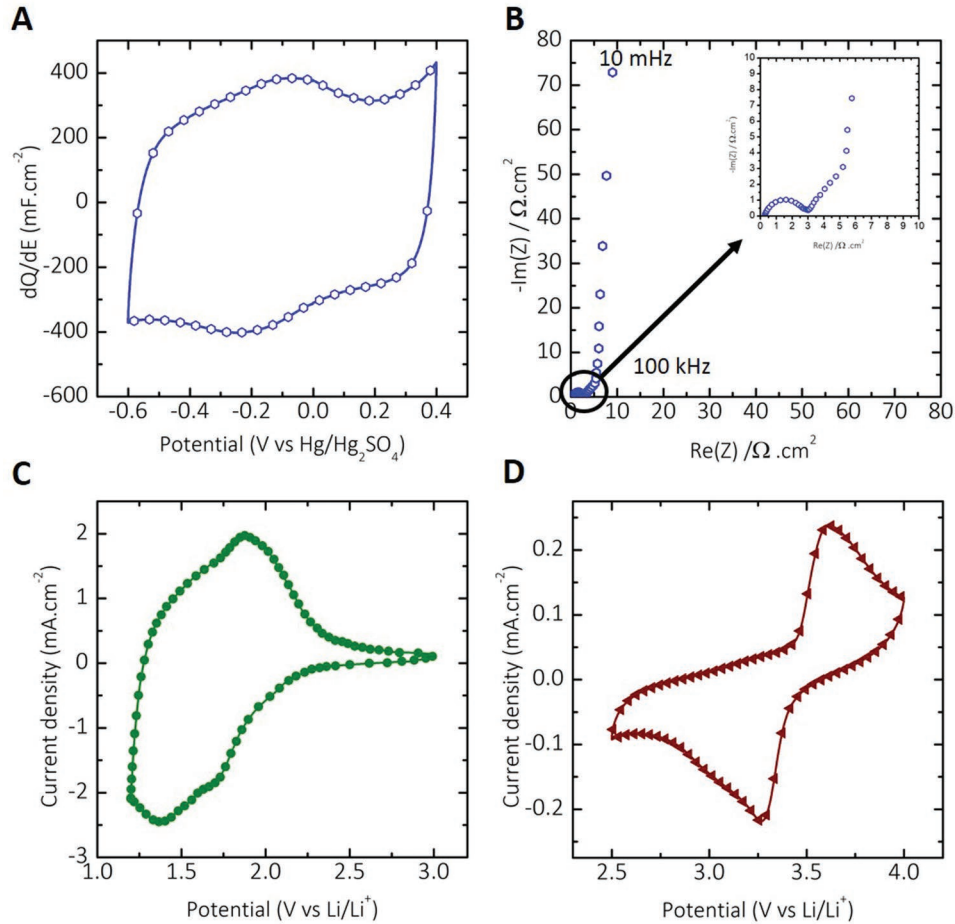


Figure 6. Versatility of the laser-writing process. A) Cyclic voltammogram recorded at 20 mV s^{-1} for a flexible carbon-based electrode obtained from the laser-writing of activated carbon and B) the corresponding Nyquist plot. C) Cyclic voltammograms recorded at 5 mV s^{-1} for flexible battery electrodes prepared by laser-writing of niobium pentoxide Nb_2O_5 and D) LiFePO_4 .

solid electrolyte was deposited on the flexible RuO_2/Au micro-supercapacitors in order to address the safety issues related to the use of liquid electrolytes. Interestingly, the cyclic voltammogram obtained with an all-solid-state microdevice (Figure 5B) is similar to the one recorded in liquid electrolyte, with only a slight decrease of capacitance (16 mF cm^{-2} at 20 mV s^{-1} against 20 mF cm^{-2} in liquid $1 \text{ M H}_2\text{SO}_4$), and an improved capacitance retention of 90% after 10 000 cycles, which is promising for the preparation of high performance all-solid-state microdevices.

2.4. Versatility of the Laser-Writing Process

The present laser-writing process is highly versatile and potentially allows the easy preparation of a broad variety of materials onto flexible substrates—since it does not depend on any laser-induced oxidation or more generally transformation of an active material precursor under the laser beam—such as activated carbon, which is commonly used in commercial ECs, as well as Nb_2O_5 , LiFePO_4 , and NiO battery materials. Indeed, the cyclic voltammogram of a laser-scribed porous activated carbon electrode (YP50F, Kuraray Co., Ltd.; see Supporting Information) recorded in $1 \text{ M H}_2\text{SO}_4$ at 5 mV s^{-1} is shown in Figure 6A.

The electrochemical signature is consistent with double layer based capacitive signature, which can be seen from the quasi-rectangular shape. Small bumps present on the CV around 0.3 V versus Ref can be attributed to pseudocapacitive contributions coming from oxygen-containing active surface groups well described in the literature.^[40] Overall, the capacitive behavior—and then the surface—of the porous carbon electrode was not significantly modified by the laser-scribing process, as confirmed by the corresponding Nyquist plot presented in Figure 6B exhibiting the migration of the ions from the electrolyte inside the electrode porosity in the middle frequency range and a typical capacitive behavior at low frequencies.^[41]

As a proof of concept, materials used in batteries were also laser-scribed directly onto flexible polyimide substrate. Negative electrodes of Nb_2O_5 (Alfa Aesar, see Supporting Information) were integrated onto polyimide by direct laser-writing of the bilayered $\text{HAuCl}_4 \cdot 3\text{H}_2\text{O}$ -cellulose acetate/ Nb_2O_5 , and tested in 1 M LiClO_4 in propylene carbonate at 5 mV s^{-1} between 2.5 V versus Li/Li^+ and 4.0 V versus Li/Li^+ . The corresponding cyclic voltammogram presented in Figure 6C exhibits a pseudocapacitive behavior typical of Nb_2O_5 ,^[42] and delivers a high areal capacitance of 180 mF cm^{-2} at 5 mV s^{-1} . LiFePO_4 positive Li-ion battery electrodes were also prepared using similar

process (see Supporting Information), and its CV is the one expected for lithium intercalation/desintercalation (Figure 6D) within the structure. Overall, that shows that the laser-writing process proposed here can be used for preparing Li-ion battery electrodes and potentially a full microbattery. This will further allow the preparation of high performance asymmetric devices operating over a larger voltage range. Finally, nickel oxide electrodes used in aqueous-based alkaline electrolyte were successfully prepared by direct laser-writing of the bilayered $\text{HAuCl}_4 \cdot 3\text{H}_2\text{O}$ -cellulose acetate/NiO deposit (Figure S11, Supporting Information). These example shows that the laser-writing process designed here allows the fabrication of a large variety of electrode and microdevices, thus making this approach very promising for the facile design of flexible microdevices in general, which will play an important role in the future to support the development of sensor networks and communicating objects.

3. Conclusion

Flexible energy microsources were successfully prepared by the simple laser-writing of commercial powders spin-coated onto raw, current-collector-free polyimide film. The use of both chloroauric acid ($\text{HAuCl}_4 \cdot 3\text{H}_2\text{O}$) and cellulose acetate as a transition layer provides heat diffusion paths in the spin-coated layer, and enabled homogeneous and adherent deposits after laser-writing. 36 RuO_2 -based micro-supercapacitors were integrated on a 10 cm-diameter polyimide foil without any short circuits. The as-prepared 500 nm-thick deposit contains Au nanoparticles disseminated in a bottom porous layer of metallic Ru and a top layer of Ru/ RuO_2 pillars which occasionally form popcorn-like structures under the laser heat. A flexible micro-supercapacitor delivering $27 \text{ mF cm}^{-2}/540 \text{ F cm}^{-3}$ in $1 \text{ M H}_2\text{SO}_4$, with a capacitance retention of 80% over 10 000 cycles, was prepared. Carbon-based electrodes were also successfully prepared, as well as battery electrodes. This laser-writing process, which does not need any mask design, mask alignment, or controlled atmosphere, paves the way for the facile and scalable fabrication of flexible micro-supercapacitors and microbatteries at large scale.

4. Experimental Section

Materials: $\text{RuO}_2 \cdot x\text{H}_2\text{O}$ was purchased from Sigma-Aldrich. Ruthenium oxide was found to be hydrated with 1.8 H_2O molecules from thermogravimetric analysis (TGA), and the size of the particles was estimated at $0.2 \mu\text{m}$ from laser diffraction scattering experiments. Chloroauric acid ($\text{HAuCl}_4 \cdot 3\text{H}_2\text{O}$) and sulfuric acid (H_2SO_4) were also purchased from Sigma-Aldrich, while Kapton foil ($75 \mu\text{m}$ -thick) was obtained from RadioSpare. A DILASE 250 UV laser (405 nm, KLOÉ, France) was used with the software KloeDesign. The laser power and writing speed were tuned to improve the adherence of the laser-scribed materials. The maximum output power was measured at 285 mW, the writing speed varies from 0.1 and 10 mm s^{-1} and the spot size is estimated at $5 \mu\text{m}$.

Electrode Preparation: A PI film was chosen for its thermal stability and low surface roughness. A Ti/Au current collector could be sputtered on the PI foil to provide a good electronic conduction during electrochemical characterizations. Then, 500 mg of cellulose acetate

were dissolved in 20 mL of THF under stirring for 1 h. Subsequently, 60 mg of $\text{HAuCl}_4 \cdot 3\text{H}_2\text{O}$ were dissolved in 0.5 mL of the cellulose acetate/THF solution, while the active material (RuO_2 powder) was dispersed in 0.5 mL of THF, and kept under sonication for 10 min. In the case of RuO_2 electrodes, the maximum amount of material to prepare homogeneous and adherent deposit was 15 mg. The $\text{HAuCl}_4 \cdot 3\text{H}_2\text{O}$ solution was first spin-coated on the PI substrate (500 rpm, 30 s). After drying in air during 2 min, the $\text{RuO}_2 \cdot x\text{H}_2\text{O}$ /THF dispersion was spin-coated using the same experimental conditions (500 rpm, 30 s). The thicknesses of the deposited coatings were 3 and $50 \mu\text{m}$, respectively. The amount of RuO_2 contained in the film was estimated at 2.05 mg cm^{-2} from inductive coupled plasma analyses (ICP, atomic emission spectroscopy). Finally, the electrodes were patterned by performing laser-writing of the homogeneous dark film with a UV laser (405 nm, power up to 285 mW, DILASE 250, KLOÉ company, France), designed for direct laser-writing. The irradiation parameters were optimized as follows: 40% of the full power (116 mW), a spot size of $5 \mu\text{m}$, a distance between two adjacent lines of $5 \mu\text{m}$ and a writing speed of $3 \pm 1 \text{ mm s}^{-1}$. The areas that were not irradiated by the laser were easily removed by washing with acetone and ethanol aliquots. Several $\text{HAuCl}_4 \cdot 3\text{H}_2\text{O}/\text{RuO}_2$ ratios (wt%) were used to study the influence of the amount of chloroauric acid on the performance of the laser-scribed RuO_2/Au electrodes.

All-Solid-State Micro-Supercapacitors: All-solid-state micro-supercapacitors were prepared by using a gel electrolyte: 1 g of PVA dissolved in 10 mL of water containing 1 mL of H_2SO_4 and kept under stirring at $85 \text{ }^\circ\text{C}$ for 3 h. Then, a drop of the solution was deposited on the devices, which were allowed to dry overnight.

Characterizations: XRD patterns of the deposits were recorded by a D4 ENDEAVOR diffractometer (Bruker, Germany) using a $\text{Cu K}\alpha$ radiation ($\lambda = 0.154 \text{ nm}$) from $2\theta = 20^\circ$ to $2\theta = 80^\circ$.

The structure of the laser-scribed RuO_2 was observed through SEM with a JSM 7100F (JEOL, Japan) with an acceleration voltage of 15.0 kV. The EDX maps have been analyzed using the AztecONE software by Oxford Instruments.

The TEM and STEM images were obtained using a probe-corrected cold-FEG JEM-ARM200F (JEOL, Japan) operated at 200 kV, equipped with an EDX. The HRTEM and SAED data were analyzed using Gatan Digital Micrograph while the EDX spectra and maps have been analyzed using JEOL Analysis station. The magnifications of TEM and STEM images have been calibrated by using monocrystalline silicon specimens.

The cross-specimen used for TEM and SEM observations was obtained using a MEB/FIB FEI HELIOS 600i equipped with a gas injection system and an EDX detector.

The electrochemical characterizations of the as-prepared electrodes were carried out using a Biologic VMP3 Potentiostat in $1 \text{ M H}_2\text{SO}_4$ in a three-electrode configuration. A $\text{Hg}/\text{Hg}_2\text{SO}_4$ electrode was used as reference electrode, and a 0.64 cm^2 Pt foil as counter electrode. The interdigitated micro-supercapacitors were tested in two-electrode configuration, by taking the electrical contacts directly on each interdigitated electrode. Cyclic voltammetry was performed at several scan rates and the areal capacitance (C , in F cm^{-2}) was calculated from Equation (1)

$$C = \frac{\int I dV}{A \cdot v \cdot \Delta V} \quad (1)$$

where I stands for the discharge current (A), v the scan rate (V s^{-1}), ΔV the potential window (V), and A the footprint area of the microdevice, including the electrodes and the electrolyte areas (cm^2).

Electrochemical impedance spectroscopy (EIS) measurements were carried out with a voltage with sinusoidal amplitude of 10.0 mV from 100 kHz to 10 MHz at the open circuit potential.

Supporting Information

Supporting Information is available from the Wiley Online Library or from the author.

Acknowledgements

The authors acknowledge support from the Chair of Excellence from the Airbus Group and ANR Labex Store Ex program. The authors are grateful to CNRS, INSA, and Université Paul Sabatier (Toulouse III) for their support and thank R. Cours for SEM observations and cross section preparation, V. Baylac for his help with the profilometer equipment, and A. Moreau for the ICP-MS measurements.

Conflict of Interest

The authors declare no conflict of interest.

Keywords

flexible micro-supercapacitors, laser-writing, ruthenium oxide

-
- [1] B. L. R. Stojkoska, K. V. Trivodaliev, *J. Cleaner Prod.* **2017**, *140*, 1454.
- [2] C. Lethien, J. Le Bideau, T. Brousse, *Energy Environ. Sci.* **2019**, *12*, 96.
- [3] M. Chan, D. Estève, J.-Y. Fourniols, C. Escriba, E. Campo, *Artif. Intell. Med.* **2012**, *56*, 137.
- [4] S. Zhai, H. E. Karahan, L. Wei, Q. Qian, A. T. Harris, A. I. Minett, S. Ramakrishna, A. K. Ng, Y. Chen, *Energy Storage Mater.* **2016**, *3*, 123.
- [5] J. R. Miller, *Science* **2012**, *335*, 1312.
- [6] J. Maeng, C. Meng, P. P. Irazoqui, *Biomed. Microdevices* **2015**, *17*, 7.
- [7] P. Simon, Y. Gogotsi, *Nat. Mater.* **2008**, *7*, 845.
- [8] K. Jost, G. Dion, Y. Gogotsi, *J. Mater. Chem. A* **2014**, *2*, 10776.
- [9] W. Liu, M.-S. Song, B. Kong, Y. Cui, *Adv. Mater.* **2017**, *29*, 1603436.
- [10] K. Jost, C. R. Perez, J. K. McDonough, V. Presser, M. Heon, G. Dion, Y. Gogotsi, *Energy Environ. Sci.* **2011**, *4*, 5060.
- [11] H. Zhang, Y. Qiao, Z. Lu, *ACS Appl. Mater. Interfaces* **2016**, *8*, 32317.
- [12] Y. Wang, Y. Shi, C. X. Zhao, J. I. Wong, X. W. Sun, H. Y. Yang, *Nanotechnology* **2014**, *25*, 094010.
- [13] H. Pang, Y. Zhang, W. Y. Lai, Z. Hu, W. Huang, *Nano Energy* **2015**, *15*, 303.
- [14] C. J. Zhang, M. P. Kremer, A. Seral-Ascaso, S. H. Park, N. McEvoy, B. Anasori, Y. Gogotsi, V. Nicolosi, *Adv. Funct. Mater.* **2018**, *28*, 1705506.
- [15] C. Guan, X. Qian, X. Wang, Y. Cao, Q. Zhang, A. Li, J. Wang, *Nanotechnology* **2015**, *26*, 094001.
- [16] T. Göhlert, P. F. Siles, T. Päßler, R. Sommer, S. Baunack, S. Oswald, O. G. Schmidt, *Nano Energy* **2017**, *33*, 387.
- [17] W. Si, C. Yan, Y. Chen, S. Oswald, L. Han, O. G. Schmidt, *Energy Environ. Sci.* **2013**, *6*, 3218.
- [18] X. Lang, A. Hirata, T. Fujita, M. Chen, *Nat. Nanotechnol.* **2011**, *6*, 232.
- [19] J. M. Sieben, E. Morallón, D. Cazorla-Amorós, *Energy* **2013**, *58*, 519.
- [20] C. Meng, J. Maeng, S. W. M. John, P. P. Irazoqui, *Adv. Energy Mater.* **2014**, *4*, 1301269.
- [21] C. B. Arnold, R. C. Wartena, K. E. Swider-Lyons, A. Pique, *J. Electrochem. Soc.* **2003**, *150*, A571.
- [22] M. F. El-Kady, V. Strong, S. Dubin, R. B. Kaner, *Science* **2012**, *335*, 1326.
- [23] J. Lin, Z. Peng, Y. Liu, F. Ruiz-Zepeda, R. Ye, E. L. G. Samuel, M. J. Yacamán, B. I. Jakobson, J. M. Tour, *Nat. Commun.* **2014**, *5*, 5714.
- [24] Z. Peng, J. Lin, R. Ye, E. L. G. Samuel, J. M. Tour, *ACS Appl. Mater. Interfaces* **2015**, *7*, 3414.
- [25] R. Q. Ye, Z. W. Peng, T. Wang, Y. N. Xu, J. B. Zhang, Y. L. Li, L. G. Nilewski, J. Lin, J. M. Tour, *ACS Nano* **2015**, *9*, 9244.
- [26] Z. Peng, R. Ye, J. A. Mann, D. Zakhidov, Y. Li, P. R. Smalley, J. Lin, J. M. Tour, *ACS Nano* **2015**, *9*, 5868.
- [27] O. Barbieri, M. Hahn, A. Foelske, R. Kotz, *J. Electrochem. Soc.* **2006**, *153*, A2049.
- [28] T. M. Dinh, A. Achour, S. Vizireanu, G. Dinescu, L. Nistor, K. Armstrong, D. Guay, D. Pech, *Nano Energy* **2014**, *10*, 288.
- [29] J. Y. Hwang, M. F. El-Kady, Y. Wang, L. Wang, Y. Shao, K. Marsh, J. M. Ko, R. B. Kaner, *Nano Energy* **2015**, *18*, 57.
- [30] J. P. Zheng, Y. Xin, *J. Power Sources* **2002**, *110*, 86.
- [31] F. X. Collard, J. Blin, *Renewable Sustainable Energy Rev.* **2014**, *38*, 594.
- [32] J. W. Chu, I. W. Shim, *J. Mol. Catal.* **1993**, *78*, 189.
- [33] K. Brousse, S. Nguyen, A. Gillet, S. Pinaud, R. Tan, A. Meffre, K. Soulantica, B. Chaudret, P. L. Taberna, M. Respaud, P. Simon, *Electrochim. Acta* **2018**, *281*, 816.
- [34] F. Wen, C. Hao, J. Xiang, L. Wang, H. Hou, Z. Su, W. Hu, Z. Liu, *Carbon* **2014**, *75*, 236.
- [35] L. Liu, D. Ye, Y. Yu, L. Liu, Y. Wu, *Carbon* **2017**, *111*, 121.
- [36] G. Lee, S.-K. Kang, S. M. Won, P. Gutruf, Y. R. Jeong, J. Koo, S.-S. Lee, J. A. Rogers, J. S. Ha, *Adv. Energy Mater.* **2017**, *7*, 1700157.
- [37] N. Kurra, B. Ahmed, Y. Gogotsi, H. N. Alshareef, *Adv. Energy Mater.* **2016**, *6*, 1601372.
- [38] N. Kurra, M. K. Hota, H. N. Alshareef, *Nano Energy* **2015**, *13*, 500.
- [39] J. Cai, C. Lv, A. Watanabe, *J. Mater. Chem. A* **2016**, *4*, 1671.
- [40] D. Hulicova-Jurcakova, M. Sereydych, G. Q. Lu, T. J. Bandoz, *Adv. Funct. Mater.* **2009**, *19*, 438.
- [41] P. L. Taberna, P. Simon, J. F. Fauvarque, *J. Electrochem. Soc.* **2003**, *150*, A292.
- [42] C. H. Lai, D. Ashby, M. Moz, Y. Gogotsi, L. Pilon, B. Dunn, *Langmuir* **2017**, *33*, 9407.